Atmos. Meas. Tech. Discuss., 6, 825–866, 2013
www.atmos-meas-tech-discuss.net/6/825/2013/
doi:10.5194/amtd-6-825-2013

Atmospheric Measurement Techniques Discussions

Impact of NO_2 horizontal heterogeneity on tropospheric NO_2 vertical columns retrieved from satellite, multi-axis differential optical absorption spectroscopy, and in situ measurements

D. Mendolia[1], R. J. C. D'Souza[1], G. J. Evans[1], and J. Brook[2]

[1]Southern Ontario Centre for Atmospheric Aerosol Research (SOCAAR), University of Toronto, 200 College St., Toronto, Ontario, Canada
[2]Environment Canada, 4905 Dufferin St., Toronto, Ontario, Canada

Received: 3 December 2012 – Accepted: 10 December 2012 – Published: 25 January 2013

Correspondence to: D. Mendolia (deanna.mendolia@utoronto.ca)

Published by Copernicus Publications on behalf of the European Geosciences Union.

Abstract

Tropospheric NO_2 vertical column densities were retrieved for the first time in Toronto, Canada using three methods of differing spatial scales. Remotely-sensed NO_2 vertical column densities, retrieved from multi-axis differential optical absorption spectroscopy and satellite remote sensing, were evaluated by comparison with in situ vertical column densities derived using a pair of chemiluminescence monitors situated 0.01 and 0.5 km above ground level. The chemiluminescence measurements were corrected for the influence of NO_z, which reduced the NO_2 concentrations at 0.01 and 0.5 km by 8 ± 1 % and 12 ± 1 %, respectively. The average absolute decrease in the chemiluminescence NO_2 measurement as a result of this correction was less than 1 ppb. Good correlation was observed between the remotely sensed and in situ NO_2 vertical column densities (Pearson R ranging from 0.68 to 0.79), but the in situ vertical column densities were 27 % to 55 % greater than the remotely-sensed columns. These results indicate that NO_2 horizontal heterogeneity strongly impacted the magnitude of the remotely-sensed columns. The in situ columns reflected an urban environment with major traffic sources, while the remotely-sensed NO_2 vertical column densities were representative of the region, which included spatial heterogeneity introduced by residential neighbourhoods and Lake Ontario. Despite the difference in absolute values, the reasonable correlation between the vertical column densities determined by three distinct methods increased confidence in the validity of the values provided by each of the methods.

1 Introduction

In Canada, nitrogen oxides (NO_x = NO + NO_2) are classified as Criteria Air Contaminants due to their adverse effects on human health and the environment (Environment Canada, 2006). Anthropogenic production of NO_x is largely attributed to fossil fuel combustion, with the transportation sector accounting for 68 % of NO_x emissions in Ontario, Canada during 2008 (MOE, 2011). NO_x emissions predominantly consist of NO, which

AMTD
6, 825–866, 2013

is oxidized to NO_2 by species such as O_3, HO_2, and RO_2. Daytime cycling between NO, NO_2, and O_3 occurs according to the photostationary state relationship, which illustrates that the steady-state concentration of O_3 is proportional to the steady-state ratio of NO_2 to NO. In the presence of volatile organic compounds (VOCs), the ratio of NO_2 to NO increases, and O_3 production is enhanced, thereby contributing to the formation of photochemical smog. O_3 production is also dependent the on ratio of NO_x present in the atmosphere relative to HO_2. Geddes et al. (2009) demonstrated that Toronto, Ontario's (43.66° N, 79.39° W) airshed exists in the NO_x-saturated regime, and as a result, O_3 production decreases with increasing NO_x concentration, since HO_x (OH + HO_2) cycling is inhibited by the chain-terminating reaction of OH with NO_2 to yield nitric acid (HNO_3) (Seinfeld and Pandis, 2006). At night, the dominant removal mechanism of NO_x is the oxidation of NO_2 by O_3 to produce the nitrate radical (NO_3). The majority of NO_3 exists as dinitrogen pentoxide (N_2O_5), which is formed via the reaction of NO_2 and NO_3. Heterogeneous reactions of N_2O_5 with aerosol to produce nitrate-bound particles serve as a major night time NO_x sink (Seinfeld and Pandis, 2006).

Previous studies investigating the spatial distribution of NO_x have focused on near-road environments as a means to assess human exposure to traffic-related air pollution (TRAP), characterize TRAP dilution and chemical evolution, inform urban infrastructure planning and policy, and validate dispersion models (Villena et al., 2011; McAdam et al., 2011; Y. Wang et al., 2011; Clements et al., 2009; Beckerman et al., 2008). These studies suggest that variability in traffic volume and fleet characteristics, as well as local topography and meteorological conditions impact the NO_x concentration (distance-decay) gradients observed amongst different near-road environments. Negative health effects associated with exposure to NO_2 when used as a marker for TRAP include the exacerbation of asthma symptoms, the increased risk of developing cardiovascular and lung diseases, and increased mortality rates. (Andersen et al., 2011; Valari et al., 2011; Pereira et al., 2010; Jerrett et al., 2009; Salam et al., 2008 and references therein; Nafstad et al., 2003). Therefore, an effective means of monitoring the spatiotemporal

AMTD
6, 825–866, 2013

behaviour of NO_2 could do much to support the development of appropriate pollution mitigation strategies.

Satellite measurements of tropospheric NO_2 vertical column densities (VCDs) can provide long-term spatiotemporal trends on a global-to-regional scale. The Ozone Monitoring Instrument (OMI) was launched onboard NASA's EOS-Aura satellite on 15 July 2004 and provides daily tropospheric NO_2 column measurements in the uv-vis spectral range of 405–465 nm with the finest resolution of $13 \times 24\,km^2$ at nadir and a local ascending equatorial crossing time of 13:45 (Levelt et al., 2006). Previous studies have extended the utility of OMI tropospheric NO_2 column measurements to validate and improve chemical transport models (e.g. S. Wang et al., 2011; X. Wang et al., 2011; Hains et al., 2010; Huijnen et al., 2010), provide top-down emission estimates of NO_x and validate bottom-up emission inventories (Shaiganfar et al., 2011; Lamsal et al., 2010), quantify long-term trends in NO_x emissions over continental source regions (Boersma et al., 2008), separate anthropogenic NO_2 emissions from biomass burning events (Mei et al., 2010), estimate the lifetime of tropospheric NO_x and account for observed seasonal patterns (Lamsal et al., 2010), infer NO_2 surface concentrations and associated long-term trends (Lee et al., 2011; Lamsal et al., 2008), and analyze the impact of precursor species on surface O_3 formation (Duncan et al., 2010). Although OMI tropospheric NO_2 columns have been applied to inform a variety of objectives, there is still a strong need for independent validation measurements (Vlemmix et al., 2010; Celarier et al., 2008; Irie et al., 2008), especially since previous validation studies have demonstrated that the relationship between OMI and field measurements varies from region-to-region (Hains et al., 2010).

On a regional and short-term scale, Ontario's Air Quality Index informs the public about their potential to experience adverse health effects from outdoor air, relying on hourly-average in situ measurements of pollutants such as NO_2, $PM_{2.5}$ and O_3 (MOE, 2010). In downtown Toronto, NO_x monitoring stations situated at 0.01 and 0.5 km above ground level (43.663° N, −79.388° W and 43.642° N, 79.387° W) provide the opportunity to derive tropospheric vertical profiles of NO_2 in a near-road

AMTD
6, 825–866, 2013

environment. Previous studies have assessed the relationship between ground-based and satellite tropospheric NO_2 VCDs, and established that VCDs derived from localised-point measurements can directly capture near-source emissions of NO_2, while the large spatial footprint ($\geq 312\,km^2$) of satellite measurements make it challenging to retrieve this information.

Petritoli et al. (2004) derived tropospheric NO_2 VCDs from ground-based in situ measurements conducted at a Po Valley background site in Gherardi, Italy during 2000–2001 using the assumption of a well-mixed planetary boundary layer, and compared these measurements to tropospheric NO_2 VCDs from the Global Ozone Monitoring Experiment. The relationship between ground-based and satellite columns exhibited seasonal differences with satellite/in situ slope ranging from 0.25 in August to 1.2 in November and December. Slopes less than 1 were shown to be dependent on the fraction of the satellite pixel's coverage of NO_2 source areas.

Ordonez et al. (2006) compared GOME satellite measurements of tropospheric NO_2 to ground-based in situ measurements of NO_2 in Lombardy, northern Italy during 1996–2002. NO_2 VCDs were derived using in situ data by using a modelled seasonal tropospheric vertical profile (using MOZART-2; spatial resolution $2.8 \times 2.8^{\circ}$). A strong agreement was seen between the measurements in relatively unpolluted areas; orthogonal regression yielded a slope near one and a correlation coefficient (R) of 0.78. However, weaker agreements were observed over polluted sites, since the horizontal resolution of GOME ($320 \times 40\,km^2$) could not isolate regions with high NO_2 concentrations.

Boersma et al. (2009) compared satellite measurements of tropospheric NO_2 from OMI to in situ-derived VCDs from 8 cities in Israel during 2006 assuming NO_2 was well-mixed in the boundary layer and negligible above this height. In situ measurement sites directly influenced by local pollutant sources showed poorest agreements with OMI observations (OMI VCD/in situ measurement orthogonal regression slopes of 0.30 and $0.59 \times 10\,molec\,cm^2\,ppb^{-1}$, and correlation coefficients of 0.65 and 0.54, respectively). Improved agreements were observed between OMI and in situ-derived VCDs from the 6 less-polluted sites (slope = 0.93; $R = 0.63$).

AMTD
6, 825–866, 2013

Multi-axis differential optical absorption spectroscopy (MAX-DOAS) is a relatively new technique used to retrieve tropospheric NO_2 columns that is well-suited for the validation of coincident OMI measurements (Halla et al., 2011; Vlemmix et al., 2010). MAX-DOAS employs intensity measurements of scattered sunlight at a series of elevation angles, relying on the narrowband absorbance structures of NO_2 within the uv/visible wavelength range, to obtain tropospheric vertical column densities (VCDs) of NO_2. Knowledge of average photon trajectories is essential for resolving NO_2 VCDs from MAX-DOAS spectra, but is an involved task, having previously been accomplished with radiative transfer modeling or trigonometric approximations. MAX-DOAS draws upon the advantages of both localised-point and satellite-based measurements, offering average pollutant concentrations covering a horizontal scale which has been reported to vary from 3 to 11 km ($\lambda =$ 357 nm, aerosol extinction coefficient within 1 km above ground level varied from 1.02 to 0.05 km^{-1}) with a time resolution on the scale of a few minutes (Irie et al., 2011).

Previous studies have investigated the relationship between OMI and MAX-DOAS tropospheric NO_2 VCDs (Shaiganfar et al., 2011; Halla et al., 2011; Wagner et al., 2010; Vlemmix et al., 2010; Kramer et al., 2008; Brinksma et al., 2008; Celarier et al., 2008; Irie et al., 2008), and demonstrated that a fair agreement was generally observed. Differences amongst the retrieved tropospheric NO_2 VCDs have been attributed to differences in the spatial resolution of ground and satellite remote sensing techniques, in addition to the vertical sensitivity of each instrument, and the NO_2 VCD retrieval algorithm employed.

The majority of studies suggest that OMI exhibits a positive bias over rural (unpolluted) MAX-DOAS measurement sites, and a negative bias over urban (polluted) MAX-DOAS measurement sites (Shaiganfar et al., 2011; Halla et al., 2011; Kramer et al., 2008; Brinksma et al., 2008; Celarier et al., 2008), despite the use of different OMI products (Standard versus DOMINO Product and versions of these products), MAX-DOAS instrumentation, and NO_2 VCD retrieval algorithms. While the OMI pixel size is $\geq$ 312 km^2, the horizontal resolution of the MAX-DOAS instrument decreases

AMTD
6, 825–866, 2013

rapidly with increasing aerosol load. Therefore, when MAX-DOAS measurements are conducted at a rural site, coincident OMI pixels may include areas with high NO_2 concentrations, and alternatively, when MAX-DOAS measurements are conducted at an urban site, coincident OMI pixels may include areas with lower NO_2 concentrations.

Previous studies have also investigated the use of stricter coincidence criterion when comparing satellite and ground-based remote sensing techniques. Brinksma et al. (2008) and Celarier et al. (2008) demonstrated that an improved agreement was observed between MAX-DOAS and OMI tropospheric NO_2 columns (increase in Pearson correlation coefficient from 0.45 to 0.65, increase in OMI/MAX-DOAS slope from 0.80 to 0.85, and decrease in OMI positive offset from 4.27 to 1.99×10^{15} molec cm^{-2}) when the MAX-DOAS VCD was averaged over several azimuths (NW, SE, SW) rather than only considering the SW azimuth. Vlemmix et al. (2010) conducted MAX-DOAS measurements at an urban location (De Bilt, Netherlands) and did not observe a significant difference between MAX-DOAS and OMI (DP v 1.02) measurements when MAX-DOAS data with a relative uncertainty $\leq 10\,\%$ was considered. Irie et al. (2008) saw an improved agreement between OMI (SP v 3) and MAX-DOAS measurements ($N = 4$; mean OMI bias $+20 \pm 8\,\%$, but within the reported OMI uncertainty) at an urban site (Tai'an, China) when the OMI pixel centre was within $0.1 \times 0.1^{\circ}$ of the MAX-DOAS measurement site, while a poor agreement was observed when the pixel centre was extended to $0.3 \times 0.3^{\circ}$ ($N = 10$; mean OMI bias $+45 \pm 38\,\%$). Shaiganfar et al. (2011) performed orthogonal regression using OMI (DP v 1.02) and mobile MAX-DOAS measurements in Delhi, India. When OMI pixels having MAX-DOAS coverage $\geq 50\,\%$ were considered, the coefficient of determination (R^2) increased from 0.48 to 0.79, but OMI pixels still exhibited a consistent negative bias.

This study examines the influence of NO_2 horizontal heterogeneity in an urban environment on VCDs determined by three methods of differing spatial scales. The goal of this study was to evaluate the response of remotely-sensed NO_2 measurements to roadside emissions of NO_2. Specifically remotely sensed tropospheric NO_2 VCD measurements from OMI (DOMINO Product, version 1.02) and MAX-DOAS were evaluated

AMTD
6, 825–866, 2013

through comparison with in situ tropospheric NO_2 VCDs, based on data collected in the downtown core of Toronto, Ontario during select periods in 2006–2010. Tropospheric NO_2 VCDs were derived using data from in situ (chemiluminescence) monitors situated near-roadside at 0.01 and 0.5 km above ground level. This is the first study that uses stationary in situ measurements of NO_2 collected near ground level to derive tropospheric NO_2 columns in an urban environment for comparison with remotely-sensed data.

MAX-DOAS NO_2 differential slant column densities (ΔSCDs) were converted to tropospheric vertical column densities (VCDs) using the geometric Air Mass Factor (AMF) approximation (Hönninger et al., 2004) in conjunction with the single-scattering validation criteria discussed by Halla et al. (2011) and Brinksma et al. (2008). The impact of NO_2 horizontal heterogeneity on the remotely-sensed VCDs was assessed by comparing MAX-DOAS and OMI tropospheric NO_2 VCDs to those derived in situ (and near-road).

This paper is structured as follows: Sect. 2 describes the methodology employed, providing an overview of the downtown Toronto measurement site, along with a description of the in situ, MAX-DOAS, and OMI instruments, and the respective NO_2 VCD retrieval algorithms. Section 3 presents the in situ-derived NO_2 VCD's seasonal trends, and the comparison between point-source and remotely sensed tropospheric NO_2 columns. Conclusions are derived based on the findings from Sect. 3, and presented in Sect. 4.

2 Methodology

2.1 Description of downtown Toronto measurement sites

In situ pollution data was obtained for the period of March 2006–March 2010 from NO_x chemiluminescence (CL), and O_3 ultraviolet photometry monitors (Thermo 42i and 49i) situated at the Ontario Ministry of the Environment (MOE) Air Quality Network's

AMTD
6, 825–866, 2013

downtown Toronto Site (DT), located 10 m above ground level (MOE, 2011b). A second set of NO_x and O_3 monitors (Thermo 49C and 42C) situated at the CN Tower (CN) sampled ambient air at 445 m above ground level and 2.3 km SSE of DT. The MOE's monitoring sites are characterized in Table 1. O_3 data was used to correct NO_2 measurements for interference from NO_z, using the procedure reported by Boersma et al. (2009), which is discussed in Sect. 2.2.

MAX-DOAS measurements were conducted at the University of Toronto's Wallberg and McLennan Physics buildings, and at Toronto's Centre Island, as summarized in Table 2. Azimuth angles were chosen based on the practical constraints of each monitoring site's topography to ensure buildings and trees did not obstruct the MAX-DOAS instrument's field of view. Both MAX-DOAS and in situ measurements of NO_2 provided the opportunity to observe the impact of diurnal traffic patterns and associated meteorology on the spatio-temporal distribution of NO_2 in an urban environment.

2.2 In situ NO_2 VCD retrieval

In situ-derived tropospheric NO_2 VCDs (NO_2 $VCD_{in\,situ}$) were calculated assuming NO_2 exhibits an exponentially decaying vertical profile, as shown in Eq. (1) where $z = 12$ km. The value selected to describe the height of the troposphere (z) made no difference to the magnitude of the VCD as $z >> H_{NO_2}$. The characteristic height of NO_2 (H_{NO_2}) was derived using the in situ NO_2 concentration at DT ($[NO_2]_{10\,m}$) and at CN ($[NO_2]_{445\,m}$), as shown in Eq. (2), where $z = 435$ m. An increase in characteristic height indicates that NO_2 occupies a greater vertical fraction of the atmosphere. NO_2 $VCD_{in\,situ}$ were calculated on a daily basis using data averaged from 12:00–14:00 EST to coincide with the OMI overpass time, and hourly-averaged NO_2 $VCD_{in\,situ}$ were also compared to coincident MAX-DOAS measurements.

$$NO_2VCD_{in\,situ} = H_{NO_2}[NO_2]_{10\,m}\left[1-\exp(-z/H_{NO_2})\right] \quad (1)$$

AMTD
6, 825–866, 2013

$$H_{NO2} = 1/\left(\frac{1}{z}\ln\frac{[NO_2]_{10\,m}}{[NO_2]_{445\,m}}\right) \quad (2)$$

Previous studies have investigated the positive bias associated with the CL detection of NO_2 due to the reduction of other oxidized nitrogen species (NO_z = nitric acid: HNO_3 + peroxy-acetyl nitrate: $C_2H_3NO_5$ + peroxyacyl nitrates: $C_xH_yO_3NO_2$ + alkyl nitrates: $RONO_2$ + nitrous acid: HONO) by the CL monitor's molybdenum (Mo) catalyst, which is unspecific to the reduction of NO_2-to-NO. The detection of NO_z is dependent on the concentration of reactive nitrogen species at the monitoring site, the relative location of emission sources, meteorology, the conversion efficiency of NO_z species by the heated molybdenum surface, and their respective line-losses (Lamsal et al., 2008 and references therein). The positive bias associated with the detection of NO_z exhibits seasonal and diurnal trends, reaching a maximum in the summer and during the afternoon when NO_z constitutes a larger fraction of NO_y (NO_z + NO_x). These trends have been associated with the photochemical production of reactive NO_z species (such as HNO_3 and PAN) alongside O_3 (Lee et al., 2011; Lamsal et al., 2008; Dunlea et al., 2007; Steinbacher et al., 2007). It was hypothesised that the bias would also vary with elevation, and thus that this positive bias should be accounted for.

The procedure reported by Boersma et al. (2009), which was based on measurements performed by Dunlea et al. (2007), was implemented to remove the influence of NO_z from CL NO_2 measurements ($[NO_2]_{CL}$) after 10:00 EST, as shown in Eq. (3), where $[NO_2]$ refers to the corrected measurement. The OMI subscript refers to the average concentration during 12:00–14:00.

$$[NO_2] = [NO_2]_{CL} - [NO_z], \quad (3)$$

where

$$[NO_z] = 0.1 \times \left([O_3] - [O_3]_{(10:00)}\right) \quad (4)$$

AMTD
6, 825–866, 2013

Boersma et al. (2009) applied Eq. (3) to correct CL NO_2 measurements at 8 cities in Israel (2006) during the OMI overpass time (13:45 LT). This reduced the CL NO_2 measurement by an average of 8 % (0.7 ppb) during 2006. This approach was validated by using the CHIMERE chemistry-transport model to determine the NO_2-to-NO_z ratio over Europe, which was typically greater than 90 % for cities exhibiting a similar NO_2 concentration as those in Israel (0–25 ppb). Boersma et al. (2009) demonstrated the NO_2-to-NO_z ratio using Eq. (3) for January, April, July, and October was 0.99, 0.98, 0.95, and 0.98, respectively, which was in excellent agreement with CHIMERE NO_2-to-NO_z ratios of 0.98, 0.96, 0.92, and 0.97. Table 3 summarizes the inclusion criteria applied to the in situ NO_2 data during March 2006–March 2010, and corresponding sample size for measurements coinciding with the OMI overpass time. Since the in situ monitors were located approximately 2.3 km apart from one another, differences in the NO_x emission characteristics at each measurement site may have influenced the observed NO_2 concentration at 10 m and 0.5 km. As shown in Table 2, the CN site experienced 24 h average weekday vehicle counts that were over 5 times greater than the DT site. Therefore, an effort was made to filter data by removing hours that were strongly influenced by horizontal NO_2 gradients, and those that did not follow a vertically decaying vertical profile. Overall, 654 of 1426 days (46 %) were maintained for further analysis.

2.3 MAX-DOAS instrument and NO_2 VCD retrieval algorithm

Measurements were conducted using a commercially available Mini-MAX-DOAS instrument developed by the Institute of Environmental Physics at the University of Heidelberg in collaboration with Hoffmann Messtechnik GmbH (Bobrowski et al., 2005). This compact unit is comprised of entrance optics, a quartz fibre bundle, a spectrograph, and Peltier cooler enclosed in an airtight metal case. The elevation angle surveyed is controlled by a stepper motor attached to the enclosed unit. The instrument is powered by a rechargeable 12 V battery, and controlled by a laptop via a USB connection.

AMTD
6, 825–866, 2013

Standalone operation of the MAX-DOAS instrument was achieved with the assistance of DOASIS software (Kraus, 2003), and entailed adjusting the appropriate jscript routine by specifying the desired series of elevation and/or azimuth angles to be surveyed. For each direction scanned, the entrance optics (a quartz lens with a field of view of 0.6° and focal length of 40 mm) collects and focuses scattered sunlight onto the attached quartz fibre bundle. Sunlight is transferred to the entrance slit of a commercial crossed Czerny-Turner Spectrograph (OceanOptics USB2000) with a linear resolution of 2048 pixels covering a wavelength range of 290–433 nm. The optical signal produced by the spectrograph is converted into a digital one via a Sony ILX511 charged-coupled device (CCD). The digital signal consists of light intensity as a function of channel (pixel) for each spectrum. This information is transferred to a laptop for future evaluation via a USB connection.

The exposure time for each spectrum was calculated by the designated jscript routine such that the CCD detector reached 80 % of its saturation level. An integrated average of 1000 spectra was used to create the final spectrum. During the hours of 09:00–16:00, the temporal resolution of measurements varied from approximately 1 to 1.5 min, mainly as a result of solar zenith angle. Around solar noon, a sequence of 6 elevation angles took approximately 8 min to survey.

"Dark current" and "offset" spectra were taken each time the instrument was set up for monitoring and subtracted from recorded spectra during analysis. The spectrometer was stabilized at 5° C for all measurements, except those conducted during the winter when the spectrometer was maintained at −5 °C to minimize the spectrometer's exposure to temperature instability.

MAX-DOAS spectra were processed with DOASIS (Kraus, 2003) and QDOAS (Fayt et al., 2011) software to retrieve NO_2ΔSCDs. Each spectrum was corrected for dark current and offset using DOASIS. The pixel-to-wavelength calibration was initially performing using a spectrum from a mercury lamp with known emission peaks. A calibration polynomial was generated in DOASIS based on the wavelength-to-pixel mapping of these peaks. QDOAS was then used to refine the wavelength calibration of each

AMTD
6, 825–866, 2013

spectrum while simultaneously characterizing the resolution (expressed as the Full-Width-Half-Maximum; FWHM) of the CCD. Each spectrum was calibrated in QDOAS by performing a non-linear least-squares fit to align the structures of the measured spectrum to those of a high-resolution solar reference spectrum (0.01 nm) (Kurucz et al., 1984) degraded to the resolution of the instrument. The resolution of the CCD (FWHM) was 0.6 nm at wavelengths greater than 380 nm.

NO_2 tropospheric ΔSCDs were retrieved from calibrated spectra by applying the DOAS technique (Platt and Stutz, 2008; Hönninger et al., 2004; Platt, 1994) using QDOAS (Fayt et al., 2011). The ΔSCD refers to the difference between the average concentration of a trace gas of interest (C) integrated along the average path length (L) traversed by photons prior to entering the spectrometer at elevation angle$_\theta$, $(\overline{CL})_\theta$or SCD_θ, and the corresponding observation at an elevation angle of 90° within a measurement cycle, $(\overline{CL})_{90°}$or $SCD_{90°}$, defined in Eqs. (3) and (4). Since the zenith spectrum within each measurement sequence was utilized as the Fraunhofer Reference Spectrum (FRS), the influence of stratospheric absorption was removed from the fit.

$$\Delta SCD = (\overline{CL})_\theta - (\overline{CL})_{90°} \quad (5)$$

$$\Delta SCD = SCD_\theta - SCD_{90°} \quad (6)$$

Fit ranges reported in numerous publications (Hönninger, 2002; Friedeburg, 2003; Wagner et al., 2004; Wittrock et al., 2004; Heckel et al., 2005; Sinreich et al., 2007; Brinksma et al., 2008) were used as guides for selecting the fit ranges used in this study. Trace gas reference spectra for NO_2 (294 K; Vandaele et al., 1996), HCHO (298 K; Meller and Moortgat, 2000), and O_3 (223 K; Bogumil et al., 2003) were convolved to the resolution of the instrument, while the O_4 cross-section (296 K; Greenblatt et al., 1990) was linearly interpolated.

Broadband absorption was accounted for by including a DOAS polynomial of order 3. A first-order offset polynomial was also used in each fit to account for stray light in the

AMTD
6, 825–866, 2013

spectrometer. The Ring Effect (Grainger and Ring, 1962) was accounted for by fitting measured spectra to a synthetic Ring spectrum generated in QDOAS by convolving a high-resolution solar spectrum (0.05 nm) (Kurucz et al., 1984b) with rotational Raman scattering cross-sections (Fayt and van Roozendael, 2001). Table 4 summarizes the fitting parameters used to retrieve the NO_2 ΔSCD.

Fitting errors associated with the MAX-DOAS ΔSCD are indicative of the systematic and random errors associated with the QDOAS retrieval. Systematic errors include incorrect spectral calibration, dark current and offset correction, and slit function characterization, as well as errors in the reference spectra, while random errors may be due to the presence of unknown spectral absorbance structures, and a low signal-to-noise ratio (Vlemmix et al., 2010; Fraser et al., 2009). The QDOAS fitting error generally increased as the magnitude of the ΔSCD decreased. With respect to NO_2, a retrieved ΔSCD of $1^{\circ}10^{17}$ molec cm^{-2} had a relative fitting error $\leq \pm 2$ %, while a retrieved ΔSCD of 2 ± 10^{15} molec cm^{-2} had a relative fitting error $\leq \pm 20$ %.

Systematic errors associated with the uncertainty, and temperature-dependence of the NO_2 absorbance cross-section have been addressed in previous studies. The measurement uncertainty associated with the NO_2 (294 K) absorption cross-section is ≤ 10 % (Vandaele et al., 1998). With respect to NO_2, Vandaele et al. (1998) observed a 20 % decrease in retrieved stratospheric NO_2 slant columns when using a NO_2 absorption cross-section measured at 220 K instead of 294 K. Vlemmix et al. (2011) demonstrated that NO_2 ΔSCDs measured using a NO_2 absorbance cross-section at 295 K should be corrected by a factor of 0.92 for an effective atmospheric temperature of 283 K (determined by considering the vertical temperature profile and the vertical distribution of NO_2 in the lower troposphere). Irie et al. (2012) reported an 11 % decrease in the NO_2 VCD by scaling it with a vertical temperature profile that decreased to 260 K at 2 km. The majority of the MAX-DOAS measurements in the current study were collected in the summer, where the characteristic height of NO_2 was typically only 500 m. Any vertical variation in the NO_2 absorbance cross-section within this region would have been small, as the relevant vertical variation of temperature was presumably

AMTD
6, 825–866, 2013

< 5°C. Thus this temperature sensitivity was not accounted for since, based on previous sensitivity studies, it would only have caused on average, an error of a few percent. Certainly, some measurements were collected in March where the average temperature was closer to 273 K and these MAX-DOAS VCDs. may be overestimated by up to 10 %.

The total uncertainty associated with the NO_2ΔSCD was calculated as the root-sum-of-squares of the QDOAS fit error, absorbance cross-section accuracy, and uncertainty associated with the temperature dependence of the differential cross-section. The total relative uncertainty of the NO_2ΔSCD varied from 15 % to 25 %. Hourly averaged NO_2ΔSCDs were calculated to convert MAX-DOAS measurements to the same timescale as in situ measurements.

Hourly averaged geometric NO_2 VCDs were determined by applying the single scattering approximation proposed by Hönninger et al. (2004) to MAX-DOAS NO_2ΔSCDs. The NO_2 differential AMF (ΔAMF = ΔSCD/VCD) was calculated as shown in Eq. (5), and verified by using the criteria NO_2 $VCD_{10°} = VCD_{20°(or\,30°)} \pm 15\,\%$ (Halla et al. 2011; Brinksma et al., 2008) to ensure tropospheric photon scattering occurred above the NO_2 column. Using this criterion resulted in 113 of the 169 available hourly MAX-DOAS NO_2ΔSCDs being excluded (Table 5). Thus, 56 h (33 %) of MAX-DOAS NO_2ΔSCDs were converted to geometric VCDs and from these time periods, 37 corresponding hours of in situ data were available for comparison.

$$\Delta\,\mathrm{AMF} = \left\langle \frac{1}{\sin\theta} - 1 \right\rangle \tag{7}$$

Previous studies have compared NO_2 VCDs retrieved using radiative transfer modeling to those calculated using the geometric ΔAMF (Wagner et al., 2010, 2011; Halla et al. 2011; Shaiganfar et al., 2011; Vlemmix et al., 2010). Wagner et al. (2011) converted NO_2 ΔSCDs measured at an elevation angle of 18° in south, north, and west viewing directions to NO_2 VCDs using the geometric approximation (VCD_{geo}) and the radiative transfer model McArtim (VCD_{RTM}; $\lambda = 360$ nm). The VCD_{geo}/VCD_{RTM} slopes were 0.88

AMTD
6, 825–866, 2013

($R^2 = 0.88$), 0.96 ($R^2 = 0.96$), and 0.92 ($R^2 = 0.86$), respectively. Although no relationship between the geometric NO_2 VCD's negative bias and aerosol optical depth (AOD) was found, this bias exhibited a systematic dependency on the vertical distribution of NO_2. This systematic dependency is anticipated since the geometric ΔAMF assumes that the tropospheric NO_2 column is contained below the last scattering altitude of photons. Wagner et al. (2011) predicted that for a NO_2 column below 1000 m, the error of the geometric NO_2 VCD is typically within 20 %.

Shaiganfar et al. (2011) demonstrated that geometric NO_2 VCDs at elevation angles of 22° and 30° differed from those determined using McArtim by ± 20 % when assuming a 500 m vertical NO_2 box profile (AOD < 1). The geometric NO_2 VCD also exhibited a systematic dependency on relative azimuth angle (difference between the solar azimuth angle and MAX-DOAS viewing direction): the geometric VCD underestimated the true VCD at low relative azimuth angles (~ 0°) and overestimated the VCD at higher relative azimuth angles (≥ 90°).

Vlemmix et al. (2010) demonstrated that, for relative azimuth angles greater than 30°, the difference between the geometric VCD at an elevation angle of 30° and McArtim VCD (λ = 428 nm) reaches a maximum of 25 %, and this offset is strongly a function of solar position relative to the MAX-DOAS instrument, as well as AOD.

The above studies did not consider the use of validation criteria in conjunction with the geometric ΔAMF to ensure the NO_2 vertical column was contained below the last scattering altitude of photons into the MAX-DOAS detector. Halla et al. (2011) compared geometrically approximated NO_2 VCDs that met the criteria $VCD_{10°} = VCD_{30°}$ (± 15 %) with those determined using the radiative transfer model McArtim (λ = 413 nm; assuming a vertical NO_2 box profile), and demonstrated geometric VCDs underestimated modeled VCDs by 8–12 %. Wagner et al. (2010) suggest that the strong agreement observed between geometrically-derived NO_2 VCDs retrieved at multiple elevation angles (22° and 40°) renders the uncertainty involved in using geometrically approximated VCDs associated with aerosol loading < 15 %. Since a similar criterion for employing the geometric ΔAMF was used in this study

AMTD
6, 825–866, 2013

(NO_2 $VCD_{10°} = VCD_{20°(or\ 30°)} \pm 15\,\%$), it is estimated that the uncertainty associated with the geometric NO_2 ΔAMF is $\leq 15\,\%$. The total relative uncertainty associated with the NO_2 VCD was calculated as the root-sum-of-squares of the random and systematic uncertainties associated with the $NO_2 \Delta SCD$ and the geometric $NO_2 \Delta AMF$. The total relative uncertainty of the MAX-DOAS NO_2 VCD retrieval ranged from 20 to 29 %.

2.4 OMI tropospheric NO_2 columns

Dutch OMI NO_2 (DOMINO Collection 3 version 1.02) tropospheric columns were obtained from the Tropospheric Emissions Monitoring Internet Service (TEMIS) (Boersma et al., 2007) for the period of March 2006–March 2010. The DOMINO Product (DP) employs the DOAS algorithm (Platt, 1994) to retrieve a NO_2 slant column density (SCD) from a measured spectrum of backscattered solar radiation for the 405–465 nm wavelength range (Bucsela et al., 2006). The stratospheric NO_2 SCD is determined by assimilating the total NO_2 SCD into the TM4 global chemistry and transport model (CTM) (Dirksen et al., 2011). The stratospheric NO_2 SCD is then subtracted from the total NO_2 SCD to determine the tropospheric SCD. The AMF is obtained from the DAK radiative transfer model (Stammes, 2001), and relies on the a-priori tropospheric NO_2 profile simulated in TM4, in addition to parameters including cloud radiance fraction, cloud pressure, surface albedo, and satellite viewing geometry. The tropospheric AMF permits the conversion of the tropospheric NO_2 SCD to the VCD (Boersma et al., 2007). Under polluted conditions, the tropospheric SCD has an absolute uncertainty of approximately 1×10^{15} molec cm^{-2} (Boersma et al., 2007, 2009), while the AMF has a relative uncertainty ranging from 10–40 % (Hains et al., 2010; Boersma et al., 2009).

The coincidence criteria used to pair OMI tropospheric NO_2 columns with independent measurements was informed by previous studies, which have constrained the sample size according to OMI cloud radiance fraction, pixel size, proximity of pixel centre to independent monitoring site, and overlap of the independent data's averaging interval with OMI overpass time (Lee et al., 2011; Hains et al., 2010; Kramer et al., 2008; Irie et al., 2008). Table 5 summarizes the criteria and coincident hours of in situ

AMTD
6, 825–866, 2013

data that were used in this study. Results are presented in this study for data that obeyed criteria 2 to 3 and 2 to 4.

Overall, of the 55 OMI overpasses with a cloud radiance fraction ≤ 0.3 and pixel centre within $0.1 \times 0.1^{\circ}$ of the MAX-DOAS measurement site, 9 coincided with MAX-DOAS NO_2 VCD measurements within ± 3 h.

3 Results and discussion

3.1 Impact of NO_z interference on chemiluminescence measurement of NO_2

Table 6 illustrates the impact of removing the NO_z interference from the CL measurement of NO_2. This correction reduced the CL NO_2 concentration at DT by 8 ± 1 % and at CN by 12 ± 1 %, suggesting, but not proving, that the need to correct for the NO_z interference associated with the CL detection of NO_2 did vary with elevation. Further, the larger NO_z interference correction at the higher elevation suggested that the correction is greater for aged air masses, consistent with observations by Boersma et al. (2009) and Steinbacher et al. (2007). The larger NO_z interference correction at the higher elevation suggests that there is a greater concentration of reactive nitrogen species at this altitude, as Dunlea et al. (2007) demonstrated that the positive and linear relationship with $[NO_z]$ and $[O_3]$ is due to the photochemical production of reactive nitrogen species alongside O_3.

The absolute decrease in the NO_2 concentration after accounting for the NO_z interference is less than 1 ppb at both DT and CN, which is similar to observations in rural Southwestern Ontario by Lee et al. (2011), who demonstrated that the median difference between the CL and true NO_2 was only 0.9 ppb. Overall, the NO_2 characteristic height decreased by an average of 30 m, and the NO_2 $VCD_{in\,situ}$ decreased by less than 1×10^{15} molec cm^{-2}.

AMTD
6, 825–866, 2013

3.2 Seasonal variation of in situ NO_2 VCD and characteristic height

The seasonal variation of the in situ derived tropospheric NO_2 VCDs is shown in Fig. 1. The monthly averaged tropospheric NO_2 VCD reaches a maximum during winter (January, February, and December), and a minimum during summer (June, July, and August). This seasonal trend is attributed to the increased photolysis during the summer. The photolysis of NO_2 decreases the concentration of NO_2 relative to NO (Seinfeld and Pandis, 2006). The increased photolysis of hydroxyl radical (OH) precursor species (such as O_3) also decreases the summertime NO_2 concentration via its reaction with OH to yield nitric acid (HNO_3) (Seinfeld and Pandis, 2006; Jacob, 1999). Furthermore, an increase in anthropogenic NO_x emissions during winter months due to residential heating may also increase the wintertime NO_2 VCD. These results are consistent with observations of seasonal NO_2 VCD trends in Lombardy, northern Italy by Ordonez et al. (2006), who combined daily ground-based in situ NO_2 concentrations with modelled tropospheric vertical profiles (using MOZART-2; spatial resolution $2.8 \times 2.8^{\circ}$).

The seasonal variation of the in situ derived NO_2 characteristic height is shown in Fig. 2. These characteristic heights for NO_2 are below the expected midday mixing height, which may reach 2 km in the summer. Overall, the NO_2 characteristic height varies insignificantly within a given season. However statistically significant differences are seen when comparing winter (colder) months to warmer months. January and February show the greatest NO_2 characteristic heights of 0.71 ± 0.08 km and 0.78 ± 0.08 km, respectively (average temperature $-2.3 \pm 1.8\,^{\circ}C$ and $-3.9 \pm 1.4\,^{\circ}C$), while minimum values are observed during the spring and summer (i.e. the characteristic height during July is 0.51 ± 0.08 km and the temperature is $24.7 \pm 0.9\,^{\circ}C$). The increased NO_2 characteristic height during colder months indicates that $[NO_2]_{(445\,m)}/[NO_2]_{(10\ m)}$ is greater during the winter than the summer, consistent with the increased lifetime of NO_2 during winter months, resulting in increased vertical homogeneity. For example, the monthly average ratio of the NO_2 concentration at 445 m to the surface, varied from 0.52 ± 0.04 during the coldest month, February

AMTD
6, 825–866, 2013

to 0.34 ± 0.04 during the warmest month, July. More generally, the monthly average $[NO_2]_{(445\,m)}/[NO_2]_{(10\,m)}$ exhibited a negative linear dependence on the monthly average temperature, with Pearson $R = 0.83$).

3.3 Comparison between in situ and remotely-sensed NO_2 VCDs

Figure 3a shows the linear regression of the OMI versus in situ tropospheric NO_2 VCD. Fig. 3b only considers a subset of these data, overpasses when the OMI pixel area was $\leq 600\,km^2$. In both figures, OMI exhibits a negative bias when compared to the in situ NO_2 VCD, however this bias decreases from 36 % to 21 %, and the Pearson R increases from 0.64 to 0.77 when a smaller OMI pixel area is considered. These results are consistent with the spatial foot print represented by these two types of measurements. The in situ monitors measure a point-location "near-roadside" NO_2 column, while the OMI NO_2 VCD reflects an average over the spatially heterogeneous Greater Toronto Area, consisting of roads, residential neighbourhoods, and Lake Ontario. Using a stricter coincidence criterion yielded an improved agreement, since a larger fraction of the OMI pixel was able to capture the downtown Toronto core.

Although version 1.02 of the DOMINO tropospheric NO_2 VCD was used for this analysis, the conclusions are anticipated to be applicable with the recently released version 2.0. Over polluted sites, DOMINO v 2.0 tropospheric NO_2 VCDs are reported to be 20 % less than the v 1.02 values during the winter, and 10 % less during the summer (Boersma et al., 2011). Of the 55 days of coincident OMI and in situ NO_2 VCDs plotted in Fig. 3b, 13 measurements are during the summer, and 15 are during the winter. The linear regression of these 28 days yield $y = 0.83x$ and $R = 0.79$, which indicates that OMI has a negative bias of 17 %, when averaged over all seasons. By scaling the winter v 1.02 NO_2 VCDs by a factor of 0.8 and the summer data by a factor of 0.9, the resulting regression is $y = 0.67x$, while the Pearson R remains unchanged. Therefore, the satellite measurement's negative bias with respect to the in-situ measurements may be larger than that suggested by Fig. 3b if DOMINO v 2.0 NO_2 VCDs are more

AMTD
6, 825–866, 2013

accurate than v1.02 values. These results would still be consistent with the spatial foot print represented by the OMI and in-situ measurements.

Figure 4 shows the linear regression results of the MAX-DOAS versus in situ tropospheric NO_2 VCD, and although a good agreement is seen (Pearson $R = 0.79$), the MAX-DOAS NO_2 VCD is only 45 % of the corresponding value determined using the in situ monitors. The difference between the MAX-DOAS versus in situ derived NO_2 VCD indicates that differences in the geographic footprint surveyed by each instrument impacted the results. As summarized in Table 2, much of the MAX-DOAS path length was over Lake Ontario during campaigns A, D and E, facing east for campaign C, and was located 65 m above ground-level in campaigns C and D. During all campaigns, the MAX-DOAS instrument's path length was also influenced by the NO_2 concentration in residential areas in the downtown core.

The spatial heterogeneity of the NO_2 concentration across Toronto was evaluated by Jerrett et al. (2007, 2009). Passive sampling measurements of NO_2 concentration at 143 sites in the early fall of 2002 and spring of 2004 were used in conjunction with land-use regression modeling to derive a NO_2 surface concentration map. Despite changes in absolute NO_2 concentration between seasons, overall spatial patterns remained similar: NO_2 exhibited higher concentrations in the west (> 20 ppb), and lower concentrations in the east (10–15 ppb). The downtown core and areas near major highways also exhibited high NO_2 concentrations (> 30 ppb). The MAX-DOAS path length over mainland Toronto consists of a combination of urban background and roadside NO_2 concentrations, and the MAX-DOAS NO_2 VCD is dependent on these gradients.

Figure 5 shows the linear regression results of OMI versus MAX-DOAS tropospheric NO_2 VCDs. A good agreement is seen between the measurement techniques, and the correlation coefficient is $R = 0.85$. The slope of 1.12 suggests that the OMI tropospheric NO_2 VCD is biased high when compared to MAX-DOAS measurements. However, this slope is not significantly different than 1.0 indicating that the OMI and MAX DOAS VCD do not differ beyond the uncertainties of these data. This slope suggests that the MAX DOAS and OMI are both "looking at" similar mixes of the spatial heterogeneity in NO_2

AMTD
6, 825–866, 2013

concentrations created by the unpolluted regions over the lake and polluted regions over the city. Thus this finding is indirectly consistent with the majority of previous studies which suggest that OMI exhibits a positive bias over rural (unpolluted) MAX-DOAS measurement sites, and a negative bias over urban (polluted) MAX-DOAS measurement sites (Shaiganfar et al., 2011; Halla et al., 2011; Wagner et al., 2010; Kramer et al., 2008; Brinksma et al., 2008; Celarier et al., 2008). In the heterogeneous polluted and unpolluted environment of the current study, the two remote sensing methods yield similar vertical columns. More importantly, when these ground and satellite based measurement methods "look at" the same mixture of environments they agree, providing reassurance in the validity of the measurements produced by each method.

The conclusions resolved from Fig. 5 should still be applicable if DOMINO version 2.0. were used instead to obtain NO_2 VCDs. Repeating the correlation shown in Fig. 5 using only the summer and winter data yields a slope of $y = 1.06x$ ($n = 8$), and a correlation coefficient of $R = 0.88$. When the winter scaling factor of 0.8 and the summer scaling factor of 0.9 (Boersma et al., 2011) are applied to the v 1.02 OMI data, the regression slope of the OMI and MAX-DOAS measurements decreases to $y = 0.88$, and the correlation coefficient is $R = 0.84$. This suggests that using an improved satellite data product may result in OMI measurements being biased low when compared to MAX-DOAS tropospheric NO_2 VCD observations. However, as discussed, in all cases the slopes are not significantly different from 1 when the uncertainties in these measurements are considered. More generally, these results are in agreement with the analysis by Irie et al. (2012), who demonstrated that the DOMINO v 2.0 tropospheric NO_2 VCD product exhibits a negative bias of 8 ± 14 % with respect to MAX-DOAS measurements, and concluded this bias to be insignificant.

4 Conclusions

In situ measurements of NO_2 in an urban environment were compared with remotely sensed satellite, and multi-axis differential optical absorption spectroscopy

AMTD
6, 825–866, 2013

(MAX-DOAS), tropospheric NO_2 vertical column densities (VCDs). The chemiluminescence measurements were first corrected for the influence of NO_z, which reduced the NO_2 concentrations at the near ground level and 445 m by 8 ± 1 % and 12 ± 1 %, respectively. The absolute decrease in the chemiluminescence NO_2 measurements as a result of this correction was less than 1 ppb.

Good agreement was observed between the remotely sensed and in situ NO_2 VCDs (Pearson R ranging from 0.64 to 0.79). However, the in situ VCDs were 27 % to 55 % greater than the remotely-sensed columns due to horizontal spatial heterogeneity. The in situ NO_2 VCD were representative of a local NO_2 column in a polluted near-road environment, while the remotely-sensed (MAX-DOAS and OMI) VCDs were representative of a spatial heterogeneous region, which included the downtown city core, residential neighbourhoods, and Lake Ontario. Overall the reasonable agreement between the VCD values determined by the three distinct methods increased confidence in the validity of the values provided by each of the methods.

Acknowledgements. The authors thank Environment Canada for funding the MAX-DOAS instrument and providing operational support for R. D'Souza. The authors acknowledge M. Van Roozendael and Caroline Fayt of the Belgian Institute for Space Aeronomy for the development of QDOAS. The authors acknowledge Stephen Kraus and Thomas Lehmann of the University of Heidelberg's Institute for Environmental Physics for the development of DOASIS. OMI NO_2 vertical column densities were retrieved by Colin Lee from the Tropospheric Emissions Monitoring Internet Service (TEMIS). The authors express their thanks to colleagues of SOCAAR, the University of Toronto's Atmospheric Physics Department, and York University's Centre for Atmospheric Chemistry for ongoing collaboration and discussions. Finally, the authors acknowledge the contribution of Sarah Basma who helped collect the Centre Island data.

AMTD
6, 825–866, 2013

References

Andersen, Z. J., Hvidberg, M., Jensen, S. S., Ketzel, M., Loft, S., Sørensen, M., Tjønneland, A., Overvad, K., and Raaschou-Nielsen, O.: Chronic obstructive pulmonary disease and long-term exposure to traffic-related air pollution: a cohort study, Am. J. Respir. Crit. Care Med., 183, 455–461, 2011.

Beckerman. B., Jerrett, M., Brook, J. R., Verma, D. K., Arain, M. A., and Finkelstein, M. A.: Correlation of nitrogen dioxide with other traffic pollutants near a major expressway, Atmos. Environ., 42, 275–290, 2008.

Bobrowski, N. and Filsinger, F.: Mini MAX-DOAS – an Introduction, Institute of Environmental Physics, University of Heidelberg, 2005.

Boersma, K. F., Eskes, H. J., Veefkind, J. P., Brinksma, E. J., van der A, R. J., Sneep, M., van den Oord, G. H. J., Levelt, P. F., Stammes, P., Gleason, J. F., and Bucsela, E. J.: Near-real time retrieval of tropospheric NO2 from OMI, Atmos. Chem. Phys., 7, 2103–2118, doi:10.5194/acp-7-2103-2007, 2007.

Boersma, K. F., Jacob, D. J., Bucsela, E. J., Perring, A. E., Dirksen, R., van der A, R. J., Yantosca, R. M., Park, R. J., Wenig, M. O., Bertram, T. H., and Cohen, R. C.: Validation of OMI tropospheric NO_2 observations during INTEX-B and application to constrain NO_x emissions over the Eastern United States and Mexico, Atmos. Environ., 42, 4480–4497, doi:10.1016/j.atmosenv.2008.02.004, 2008.

Boersma, K. F., Jacob, D. J., Trainic, M., Rudich, Y., DeSmedt, I., Dirksen, R., and Eskes, H. J.: Validation of urban NO_2 concentrations and their diurnal and seasonal variations observed from the SCIAMACHY and OMI sensors using in situ surface measurements in Israeli cities, Atmos. Chem. Phys., 9, 3867–3879, doi:10.5194/acp-9-3867-2009, 2009.

Boersma, K. F., Eskes, H. J., Dirksen, R. J., van der A, R. J., Veefkind, J. P., Stammes, P., Huijnen, V., Kleipool, Q. L., Sneep, M., Claas, J., Leitão, J., Richter, A., Zhou, Y., and Brunner, D.: An improved tropospheric NO_2 column retrieval algorithm for the Ozone Monitoring Instrument, Atmos. Meas. Tech., 4, 1905–1928, doi:10.5194/amt-4-1905-2011, 2011.

Bogumil, K., Orphal, J., Homann, T., Voigt, S., Spietz, P., Fleischmann, O. C., Vogel, A., Hartmann, M., Kromminga, H., Bovensmann, H., Frerick, J., and Burrows, J. P.: Measurements of Molecular Absorption Spectra with the SCIAMACHY Pre-Flight Model: Instrument Characterization and Reference Data for Atmospheric Remote-Sensing in the 230–2380 nm Region, J. Photochem. Photobiol. A., 157, 167–184, 2003.

AMTD
6, 825–866, 2013

Brinksma, E. J., Pinardi, G., Volten, H., Braak, R., Richter, A., Schoenhardt, A., Van Roozendael, M., Fayt, C., Hermans, C., Dirksen, R. J., Vlemmix, T., Berkhout, A. J. C., Swart, D. P. J., Oetjes, H., Wittrock, F., Wagner, T., Ibrahim, O., de Leeuw, G., Moerman, M., Curier, R. L., Celarier, E. A., Cede, A., Knap, W. H., Veefkind, J. P., Eskes, H. J., Allaart, M., Rothe, R., Piters, A. J. M., and Levelt, P. F.: The 2005 and 2006 DANDELIONS NO_2 and aerosol intercomparison campaigns, J. Geophys. Res.-Atmos., 113, D16S46, doi:10.1029/2007JD008988, 2008.

Bucsela, E. J., Perring, A. E., Cohen, R. C., Boersma, K. F., Celarier, E. A. Gleason, J. F., Wenig, M. O., Bertram, T. H., Wooldridge, P. J., Dirksen, R., and Veefkind, J. P.: Comparison of tropospheric NO_2 from in-situ aircraft measurements with near-real time and standard product data from OMI, J. Geophys. Res.-Atmos., 113, D16S31, doi:10.1029/2007JD008838, 2008.

Celarier, E. A., Brinksma, E. J., Gleason, J. F., Veefkind, J. P., Cede, A., Herman, J. R., Ionov, D., Goutail, F., Pommereau, J. P., Lambert, J. C., van Roozendael, M., Pinardi, G., Wittrock, F., Schonhardt, A., Richter, A., Ibrahim, O. W., Wagner, T., Bojkov, B., Mount, G., Spinei, E., Chen, C. M., Pongetti, T. J., Sander, S. P., Bucsela, E. J., Wenig, M. O., Swart, D. P. J., Volten, H., Kroon, M., and Levelt, P. F.: Validation of Ozone Monitoring Instrument nitrogen dioxide columns, J. Geophys. Res.-Atmos., 113, D15S15, doi:10.1029/2007JD008908, 2008.

Clements, A. L., Jia, Y., Denbleyker, A., McDonald-Buller, E., Fraser, M. P., Allen, D. T., Collins, D. R., Michel, E., Pudota, J., Sullivan, D., and Zhu, Y.: Air pollutant concentrations near three Texas roadways, Pt II, Chemical characterization and transformation of pollutants, Atmos. Environ., 43, 4523–4534, doi:10.1016/j.atmosenv.2009.06.044, 2009.

Dirksen, R. J., Boersma K. F., Eskes H. J., Ionov D. V., Bucsela E. J., Levelt P. F., and Kelder H. M.: Evaluation of stratospheric NO_2 retrieved from the Ozone Monitoring Instrument: Intercomparison, diurnal cycle, and trending, J. Geophys. Res., 116, D08305, doi:10.1029/2010JD014943, 2011.

Duncan, B. N., Yoshida, Y., Olson, J. R., Sillman, S., Martin, R. V., Lasmal, L., Hu, Y., Pickering, K. E., Retscher, C., Allen, D. J., and Crawford, J. H.: Application of OMI observations to a space-based indicator of NO_x and VOC controls on surface ozone formation, Atmos. Environ., 44, 2213–2223, doi:10.1016/j.atmosenv.2010.03.010, 2010.

Dunlea, E. J., Herndon, S. C., Nelson, D. D., Volkamer, R. M., San Martini, F., Sheehy, P. M., Zahniser, M. S., Shorter, J. H., Wormhoudt, J. C., Lamb, B. K., Allwine, E. J., Gaffney, J. S., Marley, N. A., Grutter, M., Marquez, C., Blanco, S., Cardenas, B., Retama, A., Ramos Villegas, C. R., Kolb, C. E., Molina, L. T., and Molina, M. J.: Evaluation of nitrogen dioxide

AMTD
6, 825–866, 2013

chemiluminescence monitors in a polluted urban environment, Atmos. Chem. Phys., 7, 2691–2704, doi:10.5194/acp-7-2691-2007, 2007.
Fayt, C. and Van Roozendael, M.: WinDOAS 2.1 Software User Manual, BIRA-IASB, 2001.
Fraser, A., Adams, C., Drummond, J. R., Goutail, F., Manney, G., and Strong, K.: The Polar Environment Atmospheric Research Laboratory UV-Visible Ground-Based Spectrometer: First Measurements of O_3, NO_2, BrO, and OClO Columns, J. Quant. Spectrosc. Radiat. Transfer, 110, 986–1004, doi:10.1016/j.jqsrt.2009.02.034, 2009.
Friedeburg, C.: Derivation of Trace Gas Information combining Differential Trace Gas Absorption Spectroscopy with Monte Carlo Radiative Transfer Modeling, PhD Dissertation, University of Heidelberg, Germany, 2003.
Geddes, J. A., Murphy, J. G., and Wang, D. K.: Long term changes in nitrogen oxides and volatile organic compounds in Toronto and the challenges facing local ozone control, Atmos. Environ., 43, 3407–3415, doi:10.1016/j.atmosenv.2009.03.053, 2009.
Grainger, J. F. and Ring, J.: Anomalous Fraunhofer line profiles, Nature, 193, p. 762, doi:10.1038/193762a0, 1962.
Greenblatt, G. D., Orlando, J. J., Burkholder, J. B., and Ravishankara, A. R.: Absorption measurements of oxygen between 330 and 1140 nm, J. Geophys. Res.-Atmos., 95, 18577–18582, doi:10.1029/JD095iD11p18577, 1990.
Hains, J. C., Boersma, K. F., Kroon, M., Dirksen, R. J., Cohen, R. C., Perring, A. E., Bucsela, E., Volten, H., Swart, D. P. J., Richter, A., Wittrock, F., Schonhardt, A., Wagner, T., Ibrahim, O. W., van Roozendael, M., Pinardi, G., Gleason, J. F., Veefkind, J. P., and Levelt, P.: Testing and improving OMI DOMINO tropospheric NO_2 using observations from the DANDELIONS and INTEX-B validation campaigns, J. Geophys. Res.-Atmos., 115, D05301, doi:10.1029/2009JD012399, 2010.
Halla, J. D., Wagner, T., Beirle, S., Brook, J. R., Hayden, K. L., O'Brien, J. M., Ng, A., Majonis, D., Wenig, M. O., and McLaren, R.: Determination of tropospheric vertical columns of NO_2 and aerosol optical properties in a rural setting using MAX-DOAS, Atmos. Chem. Phys., 11, 12475–12498, doi:10.5194/acp-11-12475-2011, 2011.
Heckel, A., Richter, A., Tarsu, T., Wittrock, F., Hak, C., Pundt, I., Junkermann, W., and Burrows, J. P.: MAX-DOAS measurements of formaldehyde in the Po-Valley, Atmos. Chem. Phys., 5, 909–918, doi:10.5194/acp-5-909-2005, 2005.

AMTD
6, 825–866, 2013

Hönninger, G. and Platt, U.: Observations of BrO and its vertical distribution during surface ozone depletion at Alert, Atmos. Env., 36, 2481–2489, doi:10.1016/S1352-2310(02)00104-8, 2002.

Hönninger, G., von Friedeburg, C., and Platt, U.: Multi axis differential optical absorption spectroscopy (MAX-DOAS), Atmos. Chem. Phys., 4, 231–254, doi:10.5194/acp-4-231-2004, 2004.

Huijnen, V., Williams, J. E., van Weele, M., van Noije, T. P. C., Krol, M. C., Dentener, F., Segers, A., Houweling, S., Peters, W., de Laat, A. T. J., Boersma, K. F., Bergamaschi, P., Velthoven, P. F. J., Le Sager, P., Eskes, H. J., Alkemade, F., Scheele, M. P., Nédélec, P., and Pätz, H.-W.: The global chemistry transport model TM5: description and evaluation of the tropospheric chemistry version 3.0, Geosci. Model Dev. Discuss., 3, 1009–1087, doi:10.5194/gmdd-3-1009-2010, 2010.

Irie, H., Kanaya, Y., Akimoto, H., Tanimoto, H., Wang, Z., Gleason, J. F., and Bucsela, E. J.: Validation of OMI tropospheric NO_2 column data using MAX-DOAS measurements deep inside the North China Plain in June 2006: Mount Tai Experiment 2006, Atmos. Chem. Phys., 8, 6577–6586, doi:10.5194/acp-8-6577-2008, 2008.

Irie, H., Takashima, H., Kanaya, Y., Boersma, K. F., Gast, L., Wittrock, F., Brunner, D., Zhou, Y., and Van Roozendael, M.: Eight-component retrievals from ground-based MAX-DOAS observations, Atmos. Meas. Tech., 4, 1027–1044, doi:10.5194/amt-4-1027-2011, 2011.

Irie, H., Boersma, K. F., Kanaya, Y., Takashima, H., Pan, X., and Wang, Z. F.: Quantitative bias estimates for tropospheric NO_2 columns retrieved from SCIAMACHY, OMI, and GOME-2 using a common standard for East Asia, Atmos. Meas. Tech., 5, 2403–2411, doi:10.5194/amt-5-2403-2012, 2012.

Jacob, D. J.: Introduction to Atmospheric Chemistry, Princeton University Press, Princeton N.J., 1999.

Jerrett, M., Arain, M. A., Kanaroglou, P., Beckerman, B., Crouse, D., Gilbert, N. L., Brook, J. R., Finkelstein, N., and Finkelstein, M. M.: Modeling the intraurban variability of ambient traffic pollution in Toronto, Canada. J. Toxicol. Environ. Health, Part A, 70, 200–212, 2007.

Jerrett, M., Finkelstein, M. M., Brook, J. R., Altaf Arain, M., Kanaroglou, P., Stieb, D. M., Gilbert, N. L., Verma, D., Finkelstein, N., Chapman, K. R., and Sears., M. R.: A Cohort Study of Traffic-Related Air Pollution and Mortality in Toronto, Ontario, Canada, Environ. Health Perspect., 117, 772–777, doi:10.1289/ehp.11533, 2009.

AMTD
6, 825–866, 2013

Kramer, L. J., Leigh, R. J., Remedios, J. J., and Monks, P. S.: Comparison of OMI and ground-based in situ and MAXDOAS measurements of tropospheric nitrogen dioxide in an urban area, J. Geophys. Res.-Atmos., 113, D16S39, doi:10.1029/2007JD009168, 2008.

Kraus S.: DOASUI 3.2.3268.34613, Institute of Environmental Physics – University of Heidelberg in cooperation with Hoffmann Messtichnik GmbH, www.iup.uni-heidelberg.de/bugtracker/projects/doasis/download.php/, 2003.

Kurucz, R. L., Furenlid, I., Brault, J., and Testerman, L.: Solar flux atlas from 296 nm to 1300 nm, Resolution: 0.01 nm, National Solar Observatory Atlas No 1, 1984a.

Kurucz, R. L., Furenlid, I., Brault, J., and Testerman, L.: Solar flux atlas from 296 nm to 1300 nm, Resolution: 0.05 nm, National Solar Observatory Atlas No 1, 1984b.

Lamsal, L. N., Martin, R. V., van Donkelaar, A., Steinbacher, M., Celarier, E. A., Bucsela, E., Dunlea, E. J., and Pinto, J. P.: Ground-level nitrogen dioxide concentrations inferred from the satellite-borne Ozone Monitoring Instrument, J. Geophys. Res.-Atmos., 113, D16308, doi:10.1029/2007JD009235, 2008.

Lamsal, L. N., Martin, R. V., van Donkelaar, A., Celarier, E. A., Bucsela, E. J., Boersma, K. F., Dirksen, R., Luo, C., and Wang, Y.: Indirect validation of tropospheric nitrogen dioxide retrieved from the OMI satellite instrument: insight into the seasonal variation of nitrogen oxides at northern midlatitudes, J. Geophys. Res.-Atmos., 115, D05302, doi:10.1029/2009JD013351, 2010.

Lee, C. J., Brook, J. R., Evans, G. J., Martin, R. V., and Mihele, C.: Novel application of satellite and in-situ measurements to map surface-level NO_2 in the Great Lakes region, Atmos. Chem. Phys., 11, 11761–11775, doi:10.5194/acp-11-11761-2011, 2011.

Levelt, P., van den Oord, G., Dobber, M., Malkki, A., Visser, H., de Vries, J., Stammes, P., Lundell, J., and Saari, H.: The Ozone Monitoring Instrument, IEEE T. Geosci. Remote, 44, 1093–1101, doi:10.1109/TGRS.2006.872333, 2006.

McAdam, K., Steer, P., and Perrotta, K.: Using continuous sampling to examine the distribution of traffic related air pollution in proximity to a major road, Atmos. Environ., 45, 2080–2086, doi:10.1016/j.atmosenv.2011.01.050, 2011.

Mei, L., Xue, Y., de Leeuw, G., Guang, J., Wang, Y., Li, Y., Xu, H., Yang, L., Hou, T., He, X., Wu, C., Dong, J., and Chen, Z.: Integration of remote sensing data and surface observations to estimate the impact of the Russian wildfires over Europe and Asia during August 2010, Biogeosciences, 8, 3771–3791, doi:10.5194/bg-8-3771-2011, 2011.

AMTD
6, 825–866, 2013

Meller, R. and Moortgat, G. K.: Temperature dependence of the absorption cross sections of formaldehyde between 223 and 323 K in the wavelength range 225–375 nm, J. Geophys. Res.-Atmos., 105, 7089–7101, doi:10.1029/1999JD901074, 2000.

Nafstad, P., Haheim, L. L., Oftedal, B., Gram, F., Holme, I., Hjermann, I., and Leren, P.: Lung cancer and air pollution: a 27 year follow up of 16 209 Norwegian men, Thorax., 58, 1071–107, 2003.

Ontario Ministry of the Environment (MOE): Air Quality in Ontario 2009 Report, www.ene.gov.on.ca/environment/en/resources/STDPROD_081227.html, 2011.

Ordóñez, C., Richter, A., Steinbacher, M., Zellweger, C., Nüß, H., Burrows J. P., and Prévôt, A. S. H.: Comparison of 7 years of satellite-borne and ground-based tropospheric NO_2 measurements around Milan, Italy, J. Geophys. Res.-Atmos., 111, D05310, doi:10.1029/2005JD006305, 2006.

Pereira, G., Cook, A., De Vos, A. J. B. M., and Holman, D.: A case-crossover analysis of traffic-related air pollution and emergency department presentations for asthma in Perth, Western Australia, Med. J. Australia, 193, 511–514, 2010.

Petritoli, A., Bonasoni, P., Giovanelli, G., Ravegnani, F., Kostadinov, I., Bortoli, D., Weiss, A., Schaub, D., Richter, A., and Fortezza, F.: First comparison between ground-based and satellite-borne measurements of tropospheric nitrogen dioxide in the Po basin, J. Geophys. Res.-Atmos., 109, D15307, doi:10.1029/2004JD004547, 2004.

Platt, U.: Differential Optical Absorption Spectroscopy (DOAS), Vol. 127 of Air Monitoring by Spectroscopic Technique, in: Chemical Analysis Series, edited by: John Wiley and Sons, Inc., Hoboken, NJ, USA, 27, 1994.

Platt, U. and Stutz, J.: Differential Optical Absorption Spectroscopy: Principles and Applications, Springer, Berlin, Heidelberg, Germany, 2008.

Seinfeld, J. H. and Pandis, S. N.: Atmospheric Chemistry and Physics: From Air Pollution to Climate Change 2nd Edn, John Wiley and Sons Inc., Hoboken, NJ, 2006.

Shaiganfar, R., Beirle, S., Sharma, M., Chauhan, A., Singh, R. P., and Wagner, T.: Estimation of NO_x emissions from Delhi using Car MAX-DOAS observations and comparison with OMI satellite data, Atmos. Chem. Phys., 11, 10871–10887, doi:10.5194/acp-11-10871-2011, 2011.

Sinreich, R., Friess, U., Wagner, T., and Platt, U.: Multi axis differential optical absorption spectroscopy (MAX-DOAS) of gas and aerosol distributions, Faraday Discuss., 130, 153–164, 2005.

AMTD
6, 825–866, 2013

Stammes, P.: Spectral radiance modelling in the UV-visible range, in: IRS 2000, Current problems in atmospheric radiation, edited by: Smith, W. and Timofeyev, Y. M., Deepak Publishing, Hampton, VA, 385–388, 2001.

Steinbacher, M., Zellweger, C., Schwarzenbach, B., Bugmann, S., Buchmann, B., Ordóñez, C., Prevot, A. S. H., and Hueglin, C.: Nitrogen oxide measurements at rural sites in Switzerland: bias of conventional measurement techniques, J. Geophys. Res.-Atmos., 112, D11307, doi:10.1029/2006JD007971, 2007.

Valari, M., Martinelli, L., Chatignoux, E., Crooks, J., and Garcia, V.: Time scale effects in acute association between air-pollution and mortality, Geophys. Res. Lett., 38, L10806, doi:10.1029/2011GL046872, 2008.

Vandaele, A. C., Hermans, C., Simon, P. C., Carleer, M., Colin, R., Fally, S., Merienne, M. F., Jenouvrier, A., and Coquart, B.: Measurements of the NO_2 absorption cross-section from 42 000 cm^{-1} to 10 000 cm^{-1} (238–1000 nm) at 220 K and 294 K, J. Quant. Spectrosc. Ra., 59, 171–184, 1998.

Vandaele, A. C., Hermans, C., Simon, P. C., Van Roozendael, M., Guilmot, J. M., Carleer, M., and Colin, R.: Fourier Transform Measurement of NO_2 Absorption Cross-sections in the Visible Range at Room Temperature, J. Atmos. Chem., 25, 289–305, 1996.

Villena, G., Kleffmann, J., Kurtenbach, R., Wiesen, P., Lissi, E., Rubio, M. A., Croxatto G., Rappenglück, B.: Vertical gradients of HONO, NO_x and O_3 in Santiago de Chile, Atmos. Environ., 45, 3867–3873. doi:10.1016/j.atmosenv.2011.01.073, 2011.

Vlemmix, T., Piters, A. J. M., Stammes, P., Wang, P., and Levelt, P. F.: Retrieval of tropospheric NO2 using the MAX-DOAS method combined with relative intensity measurements for aerosol correction, Atmos. Meas. Tech., 3, 1287–1305, doi:10.5194/amt-3-1287-2010, 2010.

Vlemmix, T., Piters, A. J. M., Berkhout, A. J. C., Gast, L. F. L., Wang, P., and Levelt, P. F.: Ability of the MAX-DOAS method to derive profile information for NO2: can the boundary layer and free troposphere be separated?, Atmos. Meas. Tech., 4, 2659–2684, doi:10.5194/amt-4-2659-2011, 2011.

Wagner, T., Dix, B., Friedeburg, C. v., Frieß, U., Sanghavi, S., Sinreich, R., and Platt, U.: MAX-DOAS O_4 measurements: A new technique to derive information on atmospheric aerosols – Principles and information content, J. Geophys. Res. Atmos., 109, D22205, doi:10.1029/2004JD004904, 2004.

AMTD
6, 825–866, 2013

Wagner, T., Ibrahim, O., Shaiganfar, R., and Platt, U.: Mobile MAX-DOAS observations of tropospheric trace gases, Atmos. Meas. Tech. Discuss., 2, 2851–2880, doi:10.5194/amtd-2-2851-2009, 2009.

Wang, S., Xing, J., Chatani, S., Hao, J., Klimont, Z., Cofala, J., and Amann, M.: Verification of anthropogenic emissions of China by satellite and ground observations, Atmos. Environ., 45, 6347–6358, doi:10.1016/j.atmosenv.2011.08.054, 2011.

Wang, X., Mallet, Vi., Berroir, J-P., and Herlin, I.: Assimilation of OMI NO_2 retrievals into a regional chemistry-transport model for improving air quality forecasts over Europe, Atmos. Environ., 45, 485–492, doi:10.1016/j.atmosenv.2010.09.028, 2011.

Wang, Y. J., DenBleyker, A., McDonald-Buller, E., Allen D., and Max Zhang, K.: Modeling the chemical evolution of nitrogen oxides near roadways, Atmos. Environ., 45, 43–52, doi:10.1016/j.atmosenv.2010.09.050, 2011.

Wittrock, F., Oetjen, H., Richter, A., Fietkau, S., Medeke, T., Rozanov, A., and Burrows, J. P.: MAX-DOAS measurements of atmospheric trace gases in Ny-Ålesund – Radiative transfer studies and their application, Atmos. Chem. Phys., 4, 955–966, doi:10.5194/acp-4-955-2004, 2004.

Wittrock, F., Oetjen, H., Richter, A., Fietkau, S., Medeke, T., Rozanov, A., and Burrows, J. P.: MAX-DOAS measurements of atmospheric trace gases in Ny-Ålesund – Radiative transfer studies and their application, Atmos. Chem. Phys., 4, 955–966, doi:10.5194/acp-4-955-2004, 2004.

AMTD
6, 825–866, 2013

Table 1. Location of in situ monitoring sites and pollutants of interest. *24 h average weekday vehicle counts include east and west-bound traffic (Toronto, 2010). DT refers to the Ontario Ministry of the Environment (MOE) Air Quality Network's downtown Toronto Site. CN refers to the MOE's monitoring site situated at the CN Tower.

Monitoring Site		Location	Measurement Height (m AGL)	Monitored Pollutants of Interest	Vehicle Counts (10^3 vehicles; 24-h average)*
A.	DT	Bay St./ Wellesley St. W (43.642° N, 79.387° W)	10	NO, NO_2, and O_3	17.4
B.	CN	301 Front St. W (43.663° N, 79.388° W)	445	NO, NO_2, and O_3	97.3

AMTD
6, 825–866, 2013

Table 2. Monitoring period and associated observation geometry for MAX-DOAS measurements. The horizontal distance from the MAX-DOAS instrument (at the azimuth angle surveyed) to Lake Ontario is provided in the "Mainland Toronto" column. *Campaign B surveyed 1.70 km over Lake Ontario prior to reaching mainland Toronto.

Campaign	Monitored Period	Location	Measurement Height (m AGL)	Elevation Angles of Interest (°)	Azimuth Angle (°)	Mainland Toronto (km)
A.	March 1, 3, 6–7/06	Wallberg Building (43.659° N, 79.390° W)	15	10, 20, 90	225	3.45
B.	June 13, 16–17/06	Centre Island (43.624° N, 79.365° W)	5	10, 20, 90	30	*
C.	July 18–19, 27; August 5, 8/06	McLennan Physics Building (43.660° N, 79.398° W)	65	10, 20, 90	90	10.6
D.	August 13–17/09	McLennan Physics Building	65	10, 30, 90	165	2.52
E.	March 16–19/10	Wallberg Building	15	10, 20, 30, 90	165	2.25

AMTD
6, 825–866, 2013

Table 3. In situ data selection criteria for the calculation of NO_2 $VCD_{in\,situ}$ during OMI overpass time.

	In Situ Data Selection Criteria	Days	% of Valid Data
1	Measurement Period: March 2006–March 2010	1492	
	Valid Data during March 2006–March 2010:	1426	100
2	NO, NO_2, $NO_x \geq 0$ ppb and $O_3 \geq 0$ ppb (10:00)		
3	$NO_2 \geq 0$ ppb (12:00–14:00) after applying NO_z correction	1381	97
4	Days without precipitation (rain, drizzle, or snow)	1181	83
5	NO_2 Characteristic Height (H_{NO_2}) ≥ 0 km	1051	74
6	$[NO]/[NO_2]$ 445 m < $[NO]/[NO_2]$10 m	817	57
7	Remove Outliers (exclude average H_{NO_2} data below 10th percentile and above 90th percentile); maintain 0.23 km $\leq H_{NO_2} \leq$ 1.33 km	654	46

AMTD
6, 825–866, 2013

Table 4. Summary of fit parameters employed for NO_2 ΔSCD retrieval.

Trace Gas Species of Interest	Wavelength Range (nm)	Additional Spectra Included in Fit	DOAS Polynomial Order
NO_2	405 – 431	O_4, O_3, Ring, and Offset	3

AMTD
6, 825–866, 2013

Table 5. Inclusion criteria for OMI measurements.

	OMI Overpass Inclusion Criteria	Sample Size (Number of Days)	% of Valid OMI Data
1	Overpass coincides with in situ measurement that obeys criteria in Table 3	438	
2	Cloud radiance fraction ≤ 0.3	211	48
3	Pixel centre within $0.1^\circ \times 0.1^\circ$ (≤ 10 km) of DT (43.663° N, 79.388° W)	128	28
4	Pixel Area $\leq 600\,km^2$	55	12

AMTD
6, 825–866, 2013

Table 6. Change in NO_2 concentration downtown (DT) and at the CN Tower (CN), characteristic height (H), and Vertical column density (VCD) as a result of NO_z interference correction.

Parameter	Average Relative Difference (%)	Average Absolute Difference
NO_2 DT	-8 ± 1	-0.87 ± 0.06 ppb
NO_2 CN	-12 ± 1	-0.60 ± 0.05 ppb
NO_2 H	0 ± 1	-0.03 ± 0.01 km
NO_2 VCD	-7 ± 1	$-5.38 \times 10^{14} \pm 2.66 \times 10^{14}$ molec cm^{-2}

AMTD
6, 825–866, 2013

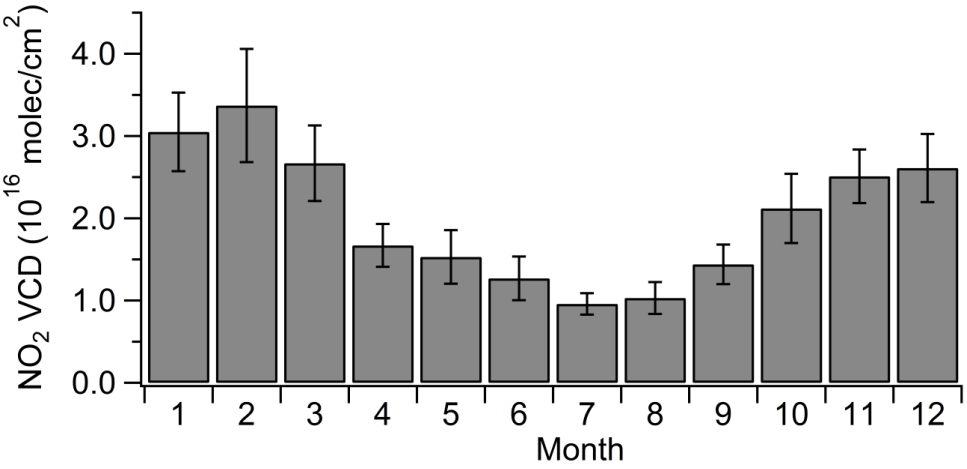

Fig. 1. Monthly averaged in situ NO_2 VCD during 12:00–14:00 EST (n = 654; Table 3).

AMTD
6, 825–866, 2013

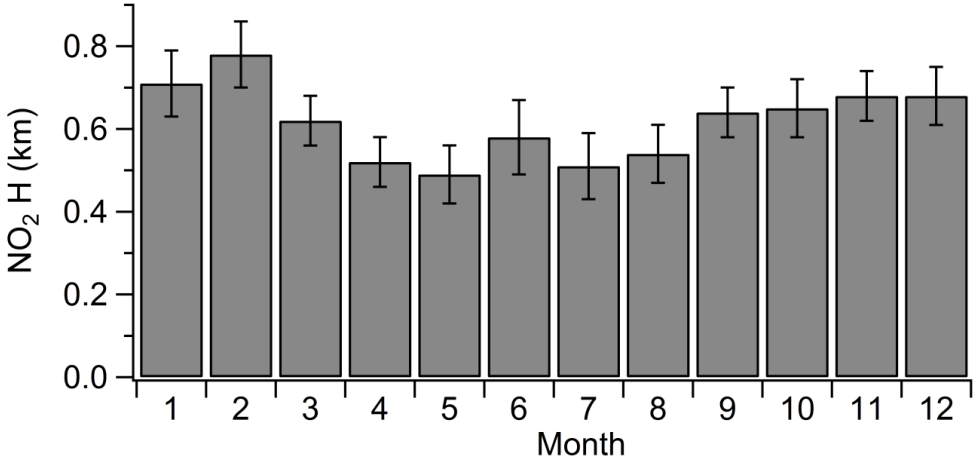

Fig. 2. Monthly averaged in situ NO_2 characteristic height during 12:00–14:00 EST (n = 654; Table 3).

AMTD
6, 825–866, 2013

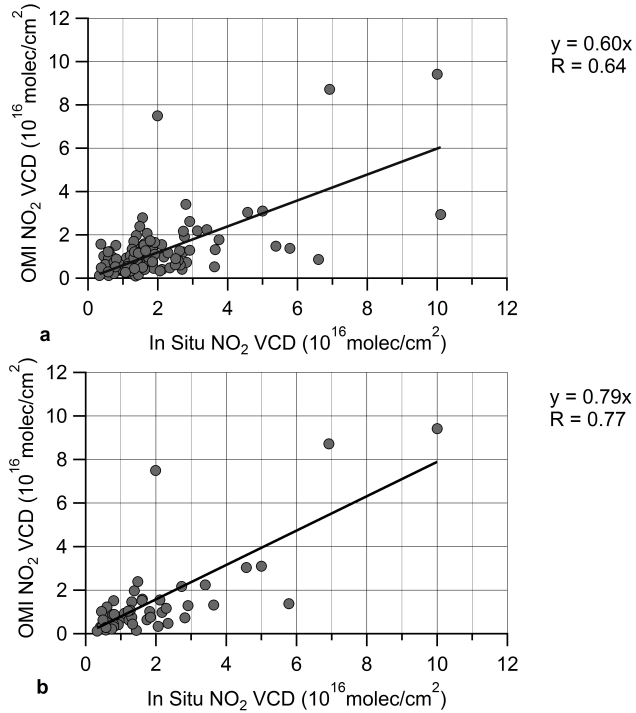

Fig. 3. (a) Linear regression of OMI versus in-situ tropospheric NO_2 VCD (n = 128; Table 5). **(b)**. Same as **(a)**. but only for overpasses with OMI pixel area ≤ 600 km (n = 55; Table 5).

AMTD
6, 825–866, 2013

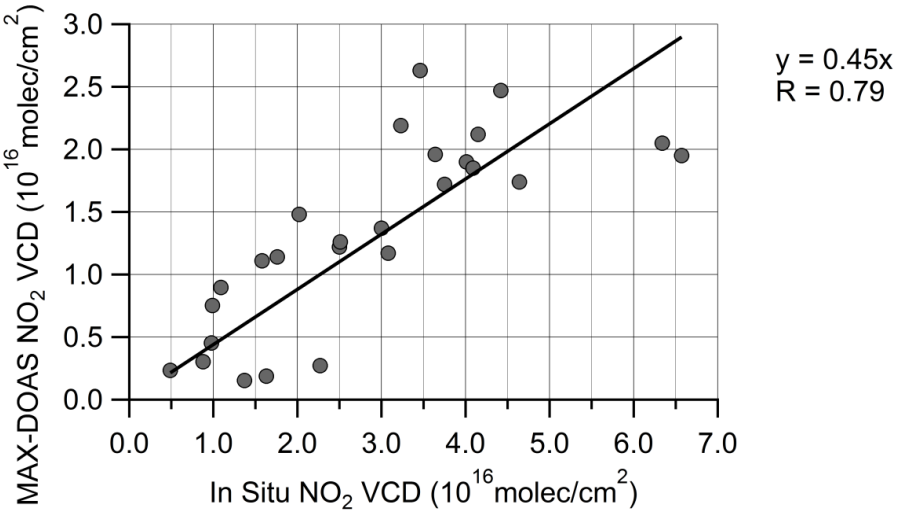

Fig. 4. Linear regression of MAX-DOAS versus in situ tropospheric NO_2 VCD (n = 56; Table 5).

AMTD
6, 825–866, 2013

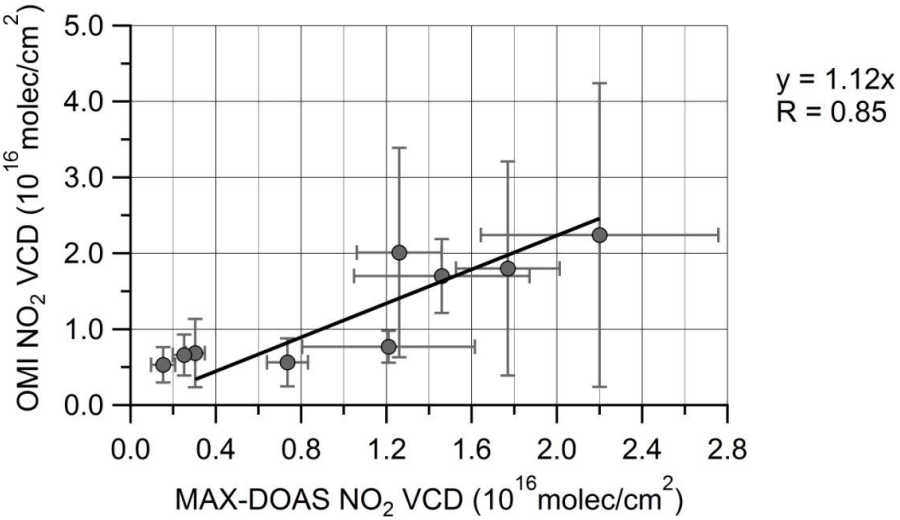

Fig. 5. Linear regression of OMI versus MAX-DOAS tropospheric NO_2 VCD (n = 9).

AMTD
6, 825–866, 2013